An assessment of the impact of local processes on dust lifting in martian climate models

Article

Supplemental Material

www.reading.ac.uk/centaur

CentAUR

Central Archive at the University of Reading

Reading's research outputs online

Supplementary Information for *An assessment of the impact of local processes on dust lifting in Martian climate models*

David P. Mulholland[1], Aymeric Spiga, Constantino Listowski and Peter L. Read

---

[1] Contact at d.p.mulholland@reading.ac.uk

1 Calculation of u_* from Mars Climate Database

1.1 Using mean u_*, z_0 (section 2.5)

The Mars Climate Database (version 5.0) contains various fields saved from model simulations run at $5.625° \times 3.75°$ horizontal resolution, with 49 vertical levels, and at 30 minutes temporal resolution (for the model physics). Using interpolation, 2-D fields can be extracted at any height, local time of day, and time of year, measured by the solar longitude, L_s. Relevant variables for the present purpose are the zonal and meridional components of the wind field, u and v, the atmospheric density, ρ, and the surface stress, τ. Additionally, for some of the variables, day-to-day temporal variability is saved in the form of a standard deviation field. The mean values result from model output that has been smoothed in time (at a fixed local time), hence the addition of the variability term is necessary to reconstruct realistic time series for each variable.

The drag velocity, u_*, can be readily obtained from the surface stress as $u_* = \sqrt{\frac{\tau}{\rho}}$. This provides the 'true' drag velocity, as calculated within the model using the variable surface stability scheme of Colaïtis et al. [2013]. However, no information on the temporal variability of τ is stored in the MCD. To create a full u_* field, temporal variability from the u and v fields at $5\,\mathrm{m}$ height is imparted to the drag velocity by generating pdfs of near-surface windspeed, and converting each of these to a drag velocity using (2), where $u(z_1) = \sqrt{u(5\,\mathrm{m})^2 + v(5\,\mathrm{m})^2}$. This conversion assumes neutral stability, so to correct for variable stability, each generated u_* value is multiplied by the ratio between true and neutral-stability mean drag velocities, $u_*/u_{*,\mathrm{neutral}}$.

2

The z_0 value used in this conversion is taken from the high-resolution roughness length map presented in section 2.1, regridded to 5° resolution. Since z_0 varies by several orders of magnitude, the geometric mean rather than the arithmetic mean is used for regridding, as this better ensures that low resolution values are not dominated by the largest-value pixels within each gridbox. The 5°-resolution z_0 map and the geometric standard deviation within each gridbox ($\sigma_g(z_0)$) are shown in Fig. S2. The 5° map is also used to calculate the threshold drag velocity, u_*^t, using (5).

Data are extracted from the MCD at 48 different local times at 30° L_s intervals, producing diurnal cycles at 30-minute resolution for 12 'months', each representing 60 sols. Probability density functions (pdfs) for u_* are generated for each month as described above, to account for daily variability within each month. Finally, monthly maximum u_* are found at the $((59/60) \times 100)^{\text{th}}$ percentile of the pdfs at each local time, and these are combined to give the annual maximum as plotted in Fig. 4.

1.2   Sub-grid sampling of u_*, z_0 (section 4)

The approach to modelling sub-grid variability in both u_* and z_0 follows the illustration shown in Fig. 10: due to the dependence of u_* on z_0, the assumed form for the wind pdf, the Weibull distribution, is applied to near-surface windspeed, $u(z_1)$, and this distribution is then converted to $u_{*,\text{sub}}$ using the method described previously. In this case, however, the $z_{0,\text{sub}}$ values used in the conversion are themselves stochastically sampled, generated with a log-normal distribution with mean equal to the 5°-gridbox-mean z_0. The two arrays are combined without any sorting, assuming that windspeed gusts occur indepen-

3

dently of roughness length variations in the underlying surface. Using the same $z_{0,\mathrm{sub}}$ distribution, a distribution of thresholds $u^t_{*,\mathrm{sub}}$ is obtained, and this is combined with the $u_{*,\mathrm{sub}}$ distribution to evaluate the dust lifting rate at each sub-grid point. The number of sub-grid points in each gridbox is defined by the critical probability, but samples of larger size (by a factor of at least ten) than this are generated, in order to accurately find the cut-off point implied by this critical probability for arrays of $u_{*,\mathrm{sub}}/u^t_{*,\mathrm{sub}}$ sorted by magnitude. For example, for a critical probability of 0.001, 10,000 values are sampled, and the largest 10 $u_{*,\mathrm{sub}}/u^t_{*,\mathrm{sub}}$ values discarded, leaving the largest acceptable value at the 99.9[th] percentile. Since the Raupach et al. [1993] drag partition function is unreliable at $z_0 > 2\,\mathrm{cm}$ (see Fig. 3), dust lifting is prohibited at any stochastically generated sub-grid points with $z_{0,\mathrm{sub}} > 2\,\mathrm{cm}$.

Two types of calculation using these fields are featured in main text: the annual maximum $u_{*,\mathrm{sub}}/u^t_{*,\mathrm{sub}}$ and the total saltation flux. The methods used for each are:

- Annual maximum: the same method as above is used to find the monthly maximum mean u_*, and from this is generated a sub-grid distribution of $u_{*,\mathrm{sub}}/u^t_{*,\mathrm{sub}}$, which is evaluated at the percentile defined by the critical probability.
- Total flux: a $u_{*,\mathrm{sub}}/u^t_{*,\mathrm{sub}}$ pdf is generated at the $(((60 - n)/60) \times 100)^{\mathrm{th}}$ percentile of the monthly mean u_* distribution, where $n = 1, 2, 3 \ldots 60$ (representing each of the 60 days in the month at a particular local time). The saltation flux is calculated for each, using (6), if $u_{*,\mathrm{sub}} > u^t_{*,\mathrm{sub}}$. In this way, monthly totals for dust flux are available, as used in Fig. 14, as well as the annual total.

4

In the dust flux calculations (Figs. 12–14), only points free from surface CO_2 ice are included.

2 Examples of stochastic sampling

Fig. S6 aims to show representative examples of the stochastic sampling method, as described in the main text, in the southern midlatitudes, with relatively strong gustiness (following Fig. S7) and with large z_0 but small $\sigma_g(z_0)$, and in the northern midlatitudes — i.e. ~ 50–$60°$N, where peak u_*/u_*^t values tend to be largest — with weaker gustiness and a smaller but more variable z_0. Although the mean windspeed lies much further below the threshold in the southern case than in the northern case, resulting dust fluxes are not greatly different. This highlights several points regarding the manner in which sub-grid scale effects control dust lifting.

Firstly, and most obviously, strong turbulent gustiness (small k) greatly enhances the potential for lifting. The southern hemisphere benefits most from this, during summer, according to Fig. S7. Secondly, roughness lengths at most gridpoints in the $5°$ map lie on the sloped part of the threshold line between $\sim 0.1\,\mathrm{cm}$ and $1\,\mathrm{cm}$, meaning that sub-grid areas with lower-than-average z_0 are preferred for lifting. Lifting rates are therefore increased by a larger spread in $z_{0,\mathrm{sub}}$ values, measured by $\sigma_g(z_0)$. The importance of z_0 variability is greatest when the sum of mean windspeed and turbulent gusts lies well below the mean threshold, as in the southern hemisphere example. The sensitivity to $\sigma_g(z_0)$ decreases when mean roughness length is decreased to $\sim 0.1\,\mathrm{cm}$, as the threshold curve flattens out at and below this value.

Finally, because of the $u_*{}^3$ term in the flux equation (6), excursions above threshold result in greater lifting rates when they occur at large z_0 (large u_* are necessarily present) than at small z_0. Therefore, such excursions may be infrequent in the southern hemisphere yet still lead to substantial dust lifting rates. This effect also leads to an increased fraction of dust lifting from rough sub-grid areas when the mean z_0 is large, counteracting the presence of the gradient in threshold (as seen in the southern hemisphere example).

The combination of these effects makes dust lifting rates more sensitive to sub-grid scale variability in the southern hemisphere ($z_0 \sim 0.5$–$1\,\mathrm{cm}$) than in smoother areas in the northern hemisphere ($z_0 \lesssim 0.3\,\mathrm{cm}$). Note that if the MacKinnon et al. [2004] drag partition function were used instead of the Raupach et al. [1993] function, the sensitivity would be reduced overall, particularly in the southern hemisphere, due to the flatter threshold curve associated with this partition function. However, dust fluxes in the southern subtropics/midlatitudes would still be the most sensitive to sub-grid variability, due to the stronger gustiness that is present in local summer, relative to northern hemispheric regions.
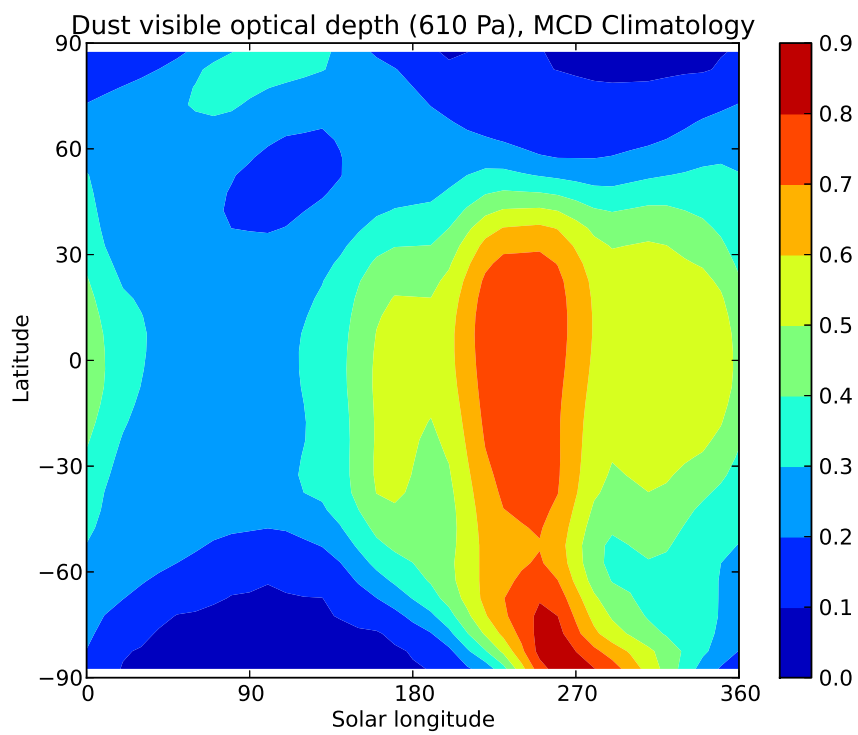
Fig. S1. Zonal-mean visible dust opacity, referenced to the $610\,\mathrm{Pa}$ level, used in the 'Climatology' scenario of the Mars Climate Database, version 5.0.
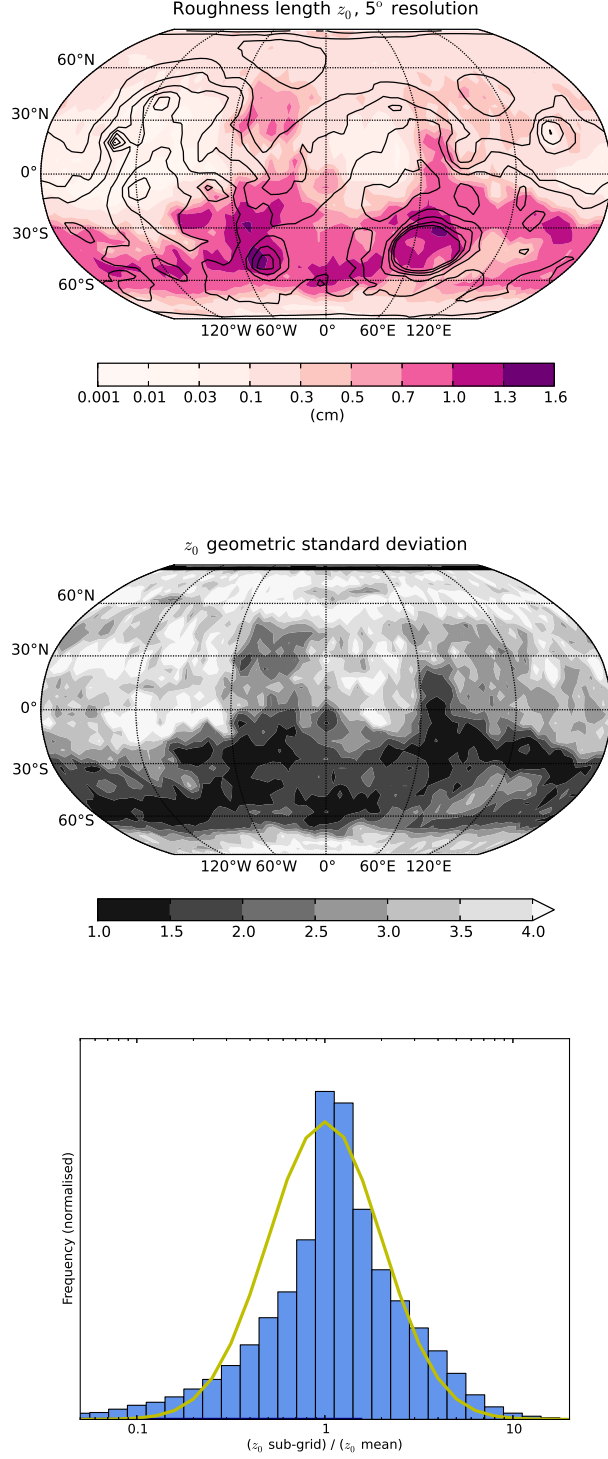
Fig. S2. (Top) Geometric mean aerodynamic surface roughness length, regridded from the high-resolution map to 5° spatial resolution; (middle) the geometric standard deviation ($\sigma_g(z_0)$); and (bottom) histogram of $\frac{1}{8}^{\circ}$ z_0 values as fractions of the mean value of the gridbox in which they are located (blue), compared to a log-normal distribution (yellow, here with the equivalent to $\sigma_g(z_0) = 2.0$) as is used in the main text (section 2 onwards) to generate $z_{0,\text{sub}}$ distributions in a gridbox with known z_0, $\sigma_g(z_0)$.
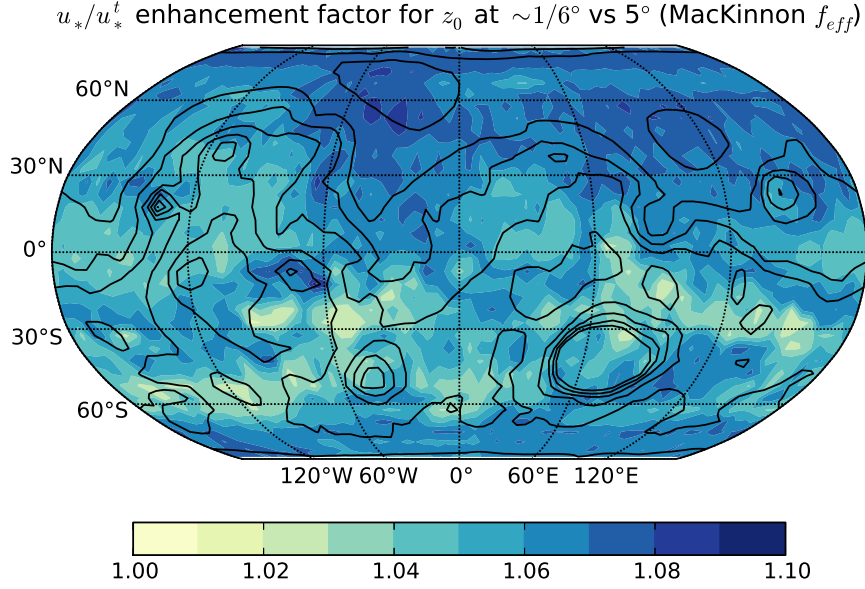
u_*/u_*^t enhancement factor for z_0 at $\sim 1/6°$ vs 5° (MacKinnon f_{eff})

Fig. S3. The ratio $\dfrac{(u_{*,\mathrm{sub}}/u_{*,\mathrm{sub}}^t)_{\max}}{u_*/u_*^t}$, for a given mean (5°) windspeed at height z_1, using the MacKinnon et al. [2004] drag partition function, and accounting for sub-grid scale z_0 variability (down to a resolution of $\sim \frac{1}{6}°$) by generating $z_{0,\mathrm{sub}}$ distributions with standard deviations σ_g to match those calculated from the full-resolution Hébrard et al. [2012] map. Note the different colour scale to Fig. 6 in the main text.
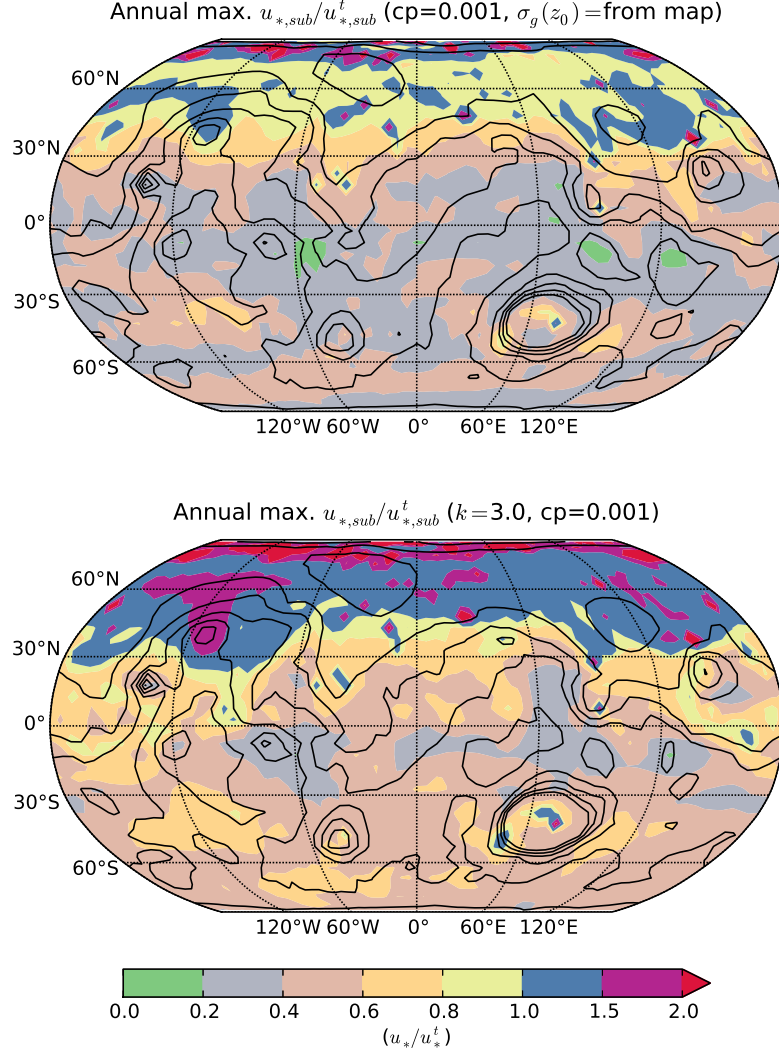
9

Fig. S4. Annual peak u_*/u_*^t with only one form of sub-grid scale variability included: z_0 variability only, using $\sigma_g(z_0)$ from the high-resolution map (top), and gustiness only, with $k = 3.0$ (bottom), each using a critical probability of 0.001.
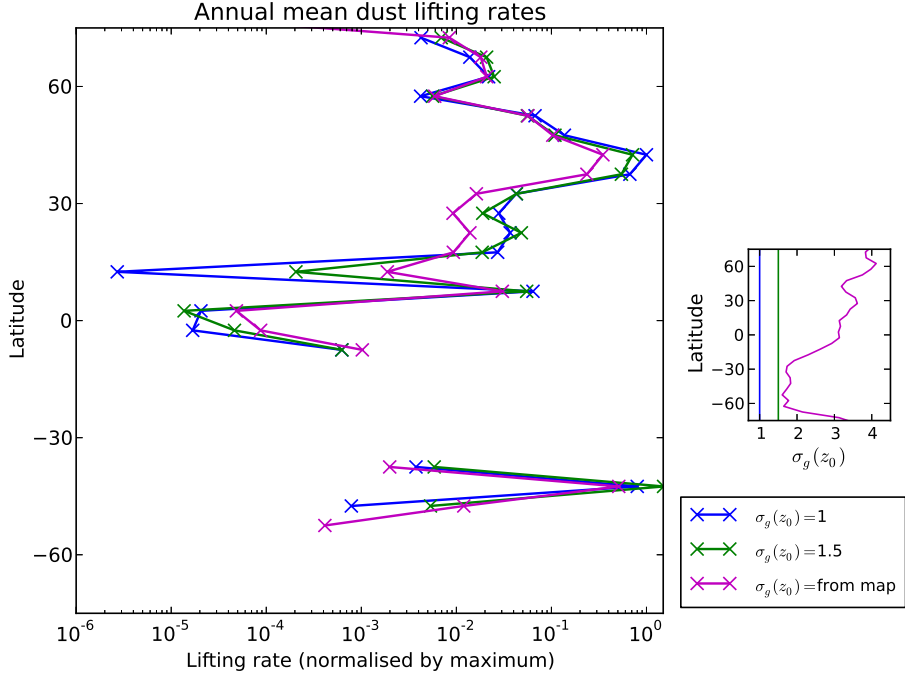
Fig. S5. Zonal-mean, annual-mean dust lifting rates $(\mathrm{g\,m^{-2}\,s^{-1}})$ from the MCD, using a Weibull distribution with $k = 3.0$ for $u(z_1)$ and a minimum probability of 0.001, for z_0 standard deviation $\sigma_g(z_0) = 1$ (blue, i.e. no variation), 1.5 (green) and taken from the high-resolution map (pink). Only ice-free gridpoints were allowed to contribute. Curves are plotted only at latitudes where some lifting occurs during the year. The zonal-mean $\sigma_g(z_0)$ obtained from the high-resolution map is shown on the right, alongside the uniform values used for the other cases. As z_0 variability is increased, lifting rates in the midlatitudes decrease: this is because wind gusts are already sufficiently large relative to the mean threshold to produce multiple lifting episodes, and any variation in z_0 introduced tends to prevent these episodes more than it encourages others, as a consequence of the $1/f_{\mathrm{eff}}$ sensitivity identified in section 2 in the main text. At latitudes less favourable for lifting, rates are increased by increasing $\sigma_g(z_0)$. So, sub-grid scale variability in roughness length can either help or hinder dust lifting, depending on the favourability of conditions for lifting otherwise.
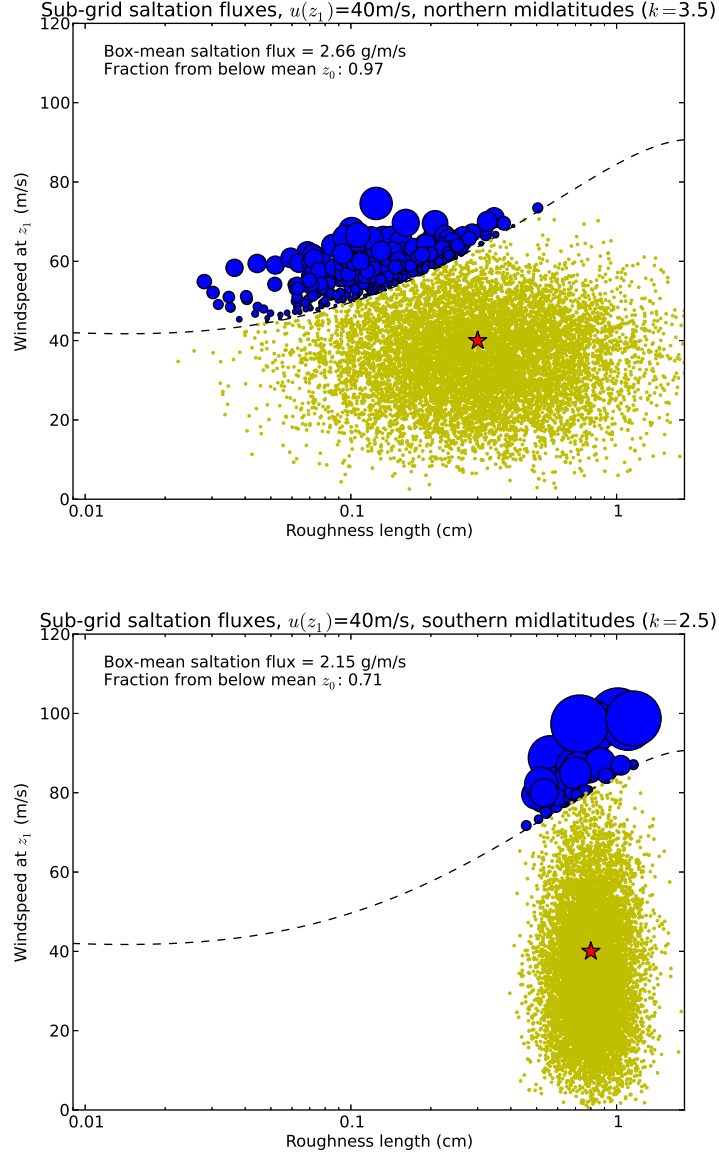
11

Fig. S6. Sub-grid saltation fluxes (calculated using equation (6) from the main text) at 10,000 sampled points within a larger gridbox (i.e. assuming a critical probability of 0.0001), in representative areas in (top) the northern midlatitudes (mean $z_0 = 0.3$ cm, $\sigma_g(z_0) = 4$, $k = 3.5$), and (bottom) the southern midlatitudes (mean $z_0 = 0.8$ cm, $\sigma_g(z_0) = 1.5$, $k = 2.5$). Red stars mark the mean conditions $(z_0, u(z_1))$ used in each case. The dashed line marks the threshold for lifting, $u(z_1)^t$. Points at which dust lifting occurs are plotted as blue circles, with sizes proportional to the local dust flux; points at which no lifting occurs are plotted as yellow dots. No lifting is permitted at points where z_0 exceeds 2 cm. The box-mean flux (to which lifting rate is proportional) is printed for each gridbox, along with the fraction of that flux that occurs at points with roughness length below the mean value. The mean windspeed applied is $40\,\mathrm{m\,s^{-1}}$ in both cases.
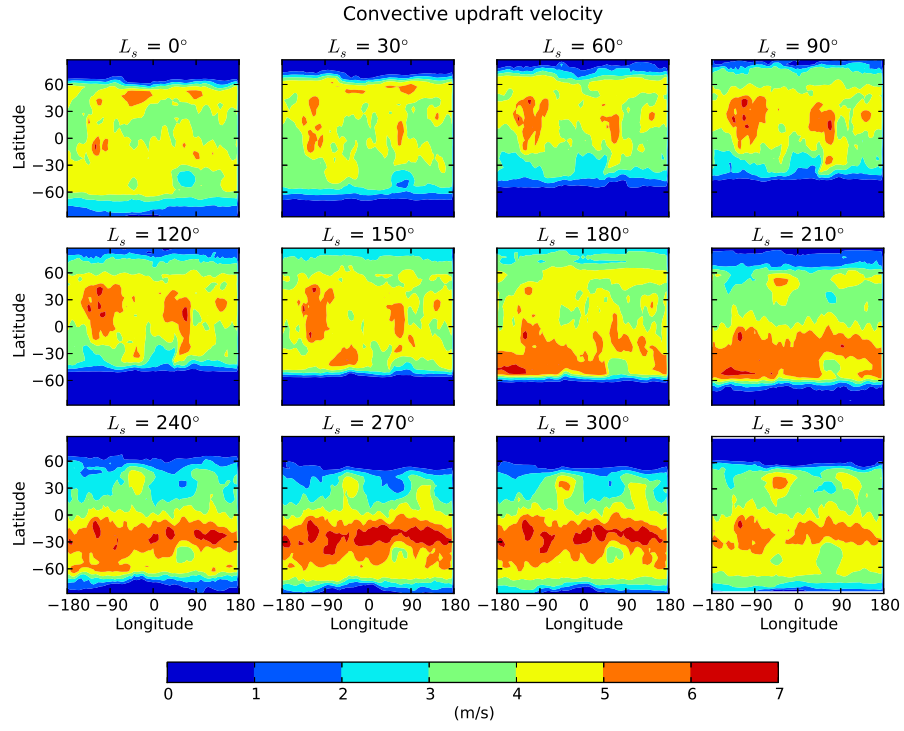
Fig. S7. Convective updraft velocity (m/s) — a proxy for turbulent gustiness — throughout a typical year, from the Climatology scenario of the MCD.